Journal of Applied Data Sciences
Vol. 5, No. 4, December 2024, pp. 1814 -1825

Biophysical Model of Mount Babaris for Predicting Carbon Potential using Remote Sensing

A. Jauhari[1,*], Isna Syauqiah[2], La Taati[3], Munsyi[4]

[1]Departement of Forestry Science, Faculty of Forestry, Lambung Mangkurat University, Banjarbaru, Indonesia

[2]Chemical Engineering Study Program, Faculty of Engineering, Lambung Mangkurat University, Banjarbaru, Indonesia

[3]Regional V Forest Area Stabilization and Environmental Management Center, Banjarbaru, Indonesia

[4]Faculty of Da'wah and Communication Science, Universitas Islam Negeri Antasari, Banjarmasin, Indonesia

(Received: July 13, 2024; Revised: July 24, 2024; Accepted: August 13, 2024; Available online: October 20, 2024)

Abstract

The biophysical model of Mount Babaris aims to predict carbon potential using remote sensing technology to address high levels of greenhouse gases, particularly CO2. This study combines satellite data with field measurements to create a validated model analyzing Forest Canopy Height (FCH), Normalized Difference Vegetation Index (NDVI), Vegetation Density (VD), and Land Surface Temperature (LST). A multiple regression analysis shows a strong correlation between these parameters and VD, with an R^2 value of 0.8673, indicating that 86.73% of the variation in vegetation density can be explained by these variables. Field validation, including drone photographs, crown and stem base density measurements, and plant size, ensures the accuracy of the satellite-derived data. The model uses the equation VD = 123.295486 x NDVI - 0.413961 x LST - 0.410253 x FCH - 3.173195, validated through field data. For processing field measurements, the equation LBDstemCor = 0.007645 x LBDcrown + 0.034348 x VD - 1.575439, with an R^2 value of 0.9564, further demonstrates its accuracy. To estimate carbon potential in kilograms per pixel (CPP), the equation CPP = LBDstemCor x FCHcor x 0.7 x 680 x 1.34 x 0.47 was used. The predicted carbon potential for Mount Babaris (1,576 ha) ranges from 607,767.55 to 607,829.54 tons, reflecting the model's precision in estimating carbon storage. This model plays a crucial role in monitoring and predicting carbon potential, supporting environmental management and climate change mitigation efforts. By integrating GIS and remote sensing, the model offers a scalable, replicable methodology adaptable to other regions with similar characteristics. It enhances the accuracy of carbon stock estimations and provides essential data for developing strategies to increase carbon sequestration, contributing to global climate change mitigation. The combination of satellite data, field measurements, and statistical analysis makes this model an invaluable tool for effective ecosystem conservation and restoration.

Keywords: Forest Planning, Biophysical Model, GreenHouse Gases, Remote Sensing, Carbon Potential

1. Introduction

Climate change occurs due to natural or human factors that alter the average climate conditions on Earth [1], [2]. One of the primary human factors is carbon emissions from the combustion of fossil fuels such as coal, petroleum, and natural gas [3]. The burning of these fossil fuels releases significant amounts of CO2, CH4, and N2O, which are potent greenhouse gases that trap heat in the atmosphere and cause global warming and climate change [4]. These excess greenhouse gases increase the Earth's surface temperature, leading to a variety of adverse effects on the environment and human societies. For instance, climate change negatively impacts agricultural productivity by reducing crop yields and raising production costs due to increased frequency and severity of extreme weather events [5], [6]. To combat these effects, adaptation and mitigation strategies have been developed, including the development of stress-resistant crop varieties, improved soil management practices, advanced irrigation techniques, and measures to reduce greenhouse gas emissions [7]. Additionally, climate change threatens biodiversity and ecosystems, as shifts in temperature and weather patterns disrupt habitats and species distributions [8], [9]. Forests play a crucial role in mitigating climate change by absorbing CO2 through photosynthesis. Approximately 50% of the carbon stored in

*Corresponding author: A. Jauhari (ajauhari@ulm.ac.id)
DOI: https://doi.org/10.47738/jads.v5i4.321

forests is contained within forest vegetation. However, activities such as forest damage, fires, logging, and deforestation release stored carbon back into the atmosphere, exacerbating the greenhouse effect [10]. The potential for CO2 absorption by forests is closely related to the availability of carbon stored in forest biomass [11]. NDVI is a valuable tool for predicting carbon potential by assessing vegetation health and density. NDVI is calculated using the reflectance of vegetation in the red and near-infrared (NIR) bands of the electromagnetic spectrum. Healthy, dense vegetation reflects more NIR and absorbs more red light, resulting in higher NDVI values. By analyzing NDVI, researchers can estimate the amount of biomass in a given area, which is directly related to the carbon stored in the vegetation. High NDVI values indicate areas with high vegetation density and, consequently, high carbon sequestration potential [11].

Many biophysical models, such as the Vegetation Index, are used to predict stand density. These models consider various factors, including species composition, soil conditions, physiography, and geography. For example, in the Western Himalayas, India, NDVI values are positively correlated with forest density ($r = 0.99$) [12]. Similarly, in Indonesia, NDVI values correlate with the density of mangrove stands in Makassar ($R = 0.943$) and vegetation in South Merapi ($r = 0.80$) [13]. Understanding the relationship between NDVI and vegetation density allows for the prediction of stand potential in other areas with similar conditions without requiring extensive field measurements [14], [15], [16], [17]. At the national level, the forestry sector in Indonesia is the largest emitter of greenhouse gases, contributing 48% of total emissions [18]. However, carbon sequestration through forestry offers significant potential to address global environmental issues, including the accumulation of greenhouse gases in the atmosphere and climate change [19], [20]. Forests absorb carbon through photosynthesis, converting light energy into chemical energy and storing it in the chemical bonds of sugars [19].

At the provincial level in South Kalimantan, information on above-ground carbon potential is still very limited and not comprehensively available. However, partial information exists regarding carbon potential in specific areas, such as the revegetation area of PT Jorong Barutama Grston, with total carbon stock in stands in 2008 amounting to 41.09 tons/ha, in 2009 to 27.43 tons/ha, and in 2010 to 22.90 tons/ha [21]. The potential for surface carbon storage is estimated at 32.03 – 46.10 tons/ha with an average of 39.06 tons/ha. PT Inhutani II Unit Semaras has a total carbon storage potential per hectare ranging from 35.48 - 51.01 tons/ha with an average of 43.24 tons/ha [22]. The provincial data for South Kalimantan is highly relevant as this region contains significant forest areas that play a crucial role in carbon sequestration. Understanding the carbon storage capacity of this region is essential for designing effective conservation and reforestation strategies, which contribute to overall climate change mitigation efforts. Moreover, this data provides a foundation for local governments to better manage forest resources and support sustainable environmental policies.

Remote sensing technology has been successfully applied in various studies to monitor and assess forest carbon stocks. For example, a study in the Amazon rainforest utilized satellite imagery to map forest biomass and carbon storage over large areas with high accuracy, demonstrating the feasibility of remote sensing for large-scale environmental monitoring. Another study in the boreal forests of Canada employed UAVs equipped with LiDAR sensors to estimate tree height and biomass, providing detailed data that enhanced forest management practices. These examples highlight the effectiveness of remote sensing technology in providing reliable, large-scale environmental data, which can be applied to similar biophysical conditions in other regions.

Existing research has rarely employed spatial modeling due to challenges such as data availability, the complexity of integrating various data sources, and the need for high-resolution imagery. These limitations make it difficult to replicate results in other areas with similar biophysical characteristics. This study aims to address these challenges by developing and implementing a spatial biophysical model that integrates satellite and field data to provide detailed and accurate information on carbon potential. The specific objectives of this study are to enhance the accuracy of carbon stock estimations, provide valuable data for developing strategies to increase carbon sequestration, and support environmental management and policy-making for climate change mitigation. By achieving these objectives, the study seeks to fill the gaps in existing research and provide a scalable and replicable methodology for other regions with similar conditions.

While studies in India and Indonesia provide valuable insights into the use of NDVI for estimating vegetation density and carbon sequestration potential, the current study at Mount Babaris seeks to expand upon these findings by incorporating a more comprehensive spatial modeling approach. The regional studies in India demonstrated a strong correlation between NDVI values and forest density, while the studies in Indonesia highlighted the relationship between NDVI and mangrove stand density. However, these studies did not fully address the integration of high-resolution satellite data with extensive field measurements, a gap that this research aims to fill. By focusing on Mount Babaris, this study will provide a more detailed and accurate assessment of carbon potential, taking into account the unique biophysical characteristics of the region. This comparison underscores the relevance and necessity of the current study in advancing our understanding of carbon sequestration in different forest ecosystems.

2. Literature Review

The use of remote sensing technology in biophysical models for predicting carbon potential has advanced significantly, especially in forest ecosystems like Mount Babaris. Tools such as NDVI, FCH, and LST have proven to be effective in estimating carbon stocks and biomass across large areas. Studies from previous research [23], [24], demonstrated that integrating remote sensing data with machine learning algorithms can improve the accuracy of carbon stock estimates, emphasizing the role of data fusion techniques such as those used by LANDSAT and GEDI (Global Ecosystem Dynamics Investigation). The research further supported this approach, showing that combining LiDAR, optical remote sensing, and machine learning enhances the precision of biomass estimation [25]. Similarly, highlighted the importance of integrating remote sensing and field data for more reliable carbon stock assessments [26]. This research also emphasized the role of multispectral and radar imagery in capturing forest structure and improving biomass predictions, especially in uneven terrains like those around Mount Babaris [27], [28]. Additionally, the researcher [29] demonstrated that combining UAV (drone) and satellite data can provide more accurate estimates of aboveground biomass in complex terrains. Reinforcement the use of NDVI and LST in assessing carbon flux across ecosystems highlighted the role of hyperspectral data in detecting subtle vegetation changes critical for carbon sequestration potential [30]. Overall, these studies underline the value of integrating advanced remote sensing technologies, as applied in the biophysical model of Mount Babaris, for accurately predicting carbon potential and supporting global climate change mitigation efforts. This body of literature reinforces the scalability and applicability of such models across diverse ecological landscapes.

3. Methodology

In this research, the methodology focuses on analyzing the biological and physical parameters of the forest land at Mount Babaris using a biophysical model to estimate wood biomass and carbon potential. Satellite data from LANDSAT-8 and Forest Canopy Height data are combined with field surveys to create a comprehensive dataset. The field data includes drone images, tree coordinates, dimensions, and density measurements. A cluster method is used to select sample areas, categorizing the forest into very low, low, and medium-density zones, with 23 plots sampled. The collected data is processed to calculate parameters such as NDVI, LST, and vegetation density, which are then analyzed using regression models.

3.1. Study Area

The research was conducted on Mount Babaris which is the location of the forestry faculty's educational forest, Gulung Mangkurat University, South Kalimantan, Indonesia covering an area of 1,576 ha. The forest on Mount Babaris is a forest dominated by secondary forest.

3.2. Data Collection Technique

This research involves field surveys and satellite data processing. The satellite data used are remote sensing data. The satellite data utilized includes LANDSAT-8 coverage for the year 2021 and plant canopy height satellite data for the year 2019. The satellite data is processed first to obtain initial density conditions. Parameters analyzed for satellite data include FCH, NDVI, VD, and LST. Field data comprises Drone Photos, tree location coordinates, tree dimensions, and stem and crown base density.

3.3. Sampling Area

A cluster method is applied to the stand density parameter to determine the sampling area locations. There are three main clusters: very low, low, and medium density. Sample areas are determined using purposive plot sampling in each

Journal of Applied Data Sciences
Vol. 5, No. 4, December 2024, pp. 1814 -1825

of the created clusters. The sampling plot size is 30x30m. A total of 23 sampling plots are distributed across all the main clusters. The stand density map and sample locations are presented in figure 1 below.

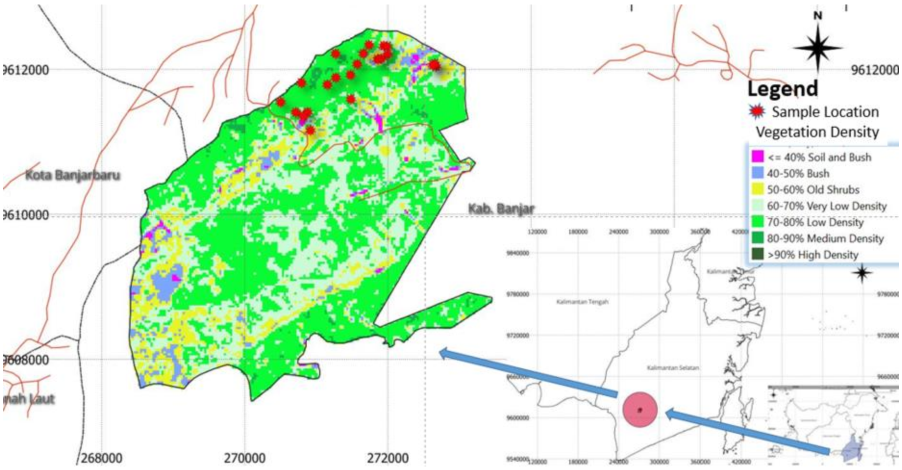

Figure 1. Vegetation Density and Sampling Plot Location Map

In conducting data sampling analysis, several formulas in this research are used to calculate and analyze the sampling data obtained from satellite imagery, which is then processed using remote sensing technology [31]. The formulas used are as follows:

The formulas used to calculate NDVI with LANDSAT satellite data are as follows:

$$\text{NDVI} = \frac{\text{NIR}-\text{R}}{\text{NIR}+\text{R}} \tag{1}$$

Note: NDVI = Normalized Difference Vegetation Index; NIR = Near Infrared; R = Red

VD Based on Basal Area:

$$\text{VD} = \sum_{i=1}^{n}\left(\frac{\pi \times \text{DBH}_i^2}{4}\right) \tag{2}$$

Note: VD is Vegetation Density in m² per hectare; DBHi is the Diameter at Breast Height of the i-th tree;

LST:

The general steps to calculate LST from Landsat 8 satellite data are as follows:

Convert Digital Number (DN) to Radiance:

$$[\, L_\lambda = \frac{(L_{max} - L_{min})}{Q_{max} - L_{min}} \times (Q_{cal} - L_{min}) + L_{min} \,] \tag{3}$$

Convert Radiance to Brightness Temperature:

$$[\, T_B = \frac{K_2}{\ln\left(\frac{K_1}{L_\lambda} + 1\right)} \,] \tag{4}$$

Note: T_B is the brightness temperature in Kelvin; K_1 and K_2 are the thermal sensor calibration constants.

Emissivity Correction:

Emissivity (ε) is a factor that accounts for the efficiency of the surface in emitting thermal radiation. Emissivity for vegetation and soil varies and is typically determined based on NDVI.

Convert Brightness Temperature to LST:

ISSN 2723-6471

$$[\, LST = \frac{T_B}{1 + (\lambda \times T_B / \rho) \times \ln L\ \varepsilon} \,] \tag{5}$$

Note: λ is the wavelength of thermal radiation.

$$\rho = (\frac{h \times c}{s})\ \text{adalah konstanta}\ (1.438 \times 10^{-}2\ \text{m K}) \tag{6}$$

ε is the surface emissivity.

Calculation of Stand Volume:

$$V = 0,25 \times \pi \times (\frac{D}{100})2 \times t \times f \tag{7}$$

Note: V = Volume (m^2); π = Pi (3.14); D = Diameter (m); t = Height (m); f = Tree form factor (0.7)

Calculation of Stand Biomass:

$$B = LBD \times Height \times 0.7 \times WD \times BEF \tag{8}$$

Note: B = Biomass (kg); LBD = Basal Area (m^2); WD = Wood density (kg/m^3) (the WD value for forest wood is 680 kg/m^3) BEF = Biomass expansion factor (the BEF value for forest wood is 1.34)

Calculation of Understory and Litter Biomass:

$$BKT = BKC / BBC \times BBT \tag{9}$$

Note: BKT = Total Dry Weight (g); BKC = Sample Dry Weight (g); BBC = Sample Wet Weight (g); BBT = Total Wet Weight (g)

Calculation of Carbon Stock:

$$C = B \times 0.47 \tag{10}$$

Note: C = Carbon Stock (kg); B = Biomass (kg); 0.47 = Percentage of carbon in organic matter (BSN 2011)

Calculation of Carbon Stock per Hectare:

$$Cn = \frac{Cx}{1000} \times \frac{10000}{L.Plot} \tag{11}$$

Note: Cn = Estimated total carbon stock (tons/ha); Cx = Carbon stock value per plot (kg); L_Plot = Observation plot area (m^2)

Calculation of CO2 Sequestration:

$$CO2 = Cn \times 3.67 \tag{12}$$

Note: CO2 = CO2 Sequestration (tons/ha); Cn = Estimated total carbon stock (tons/ha); 3.67 = Carbon conversion factor.

3.4. Research Procedure

The data processing stages in this research can be seen graphically in figure 2 below. From figure 2, the research begins with downloading LANDSAT-8 data and FCH data from the Global Ecosystem Dynamics Investigation (GEDI). The initial data for the biophysical model is entirely sourced from satellite data, including LANDSAT-8 and GEDI. The downloaded data are then corrected both geographically and radiometrically to ensure accuracy. Once corrected, the data are processed to obtain NDVI, VD, and LST. To focus on the specific region of Mount Babaris, the study area is masked accordingly. Simple regression is initially performed using VD, NDVI, FCH, and LST. If the R^2 value from the simple regression is greater than 0.3, the process advances to multiple regression analysis. If the multiple regression analysis yields an R^2 value greater than 0.8, a VD map of Mount Babaris is created. This is followed by clustering and purposive plot sampling to prepare for field data collection. After these preparations, a field survey is conducted using the purposive cluster plot sampling method. During the field survey, data such as the coordinates and dimensions of trees within each sampling plot are collected.

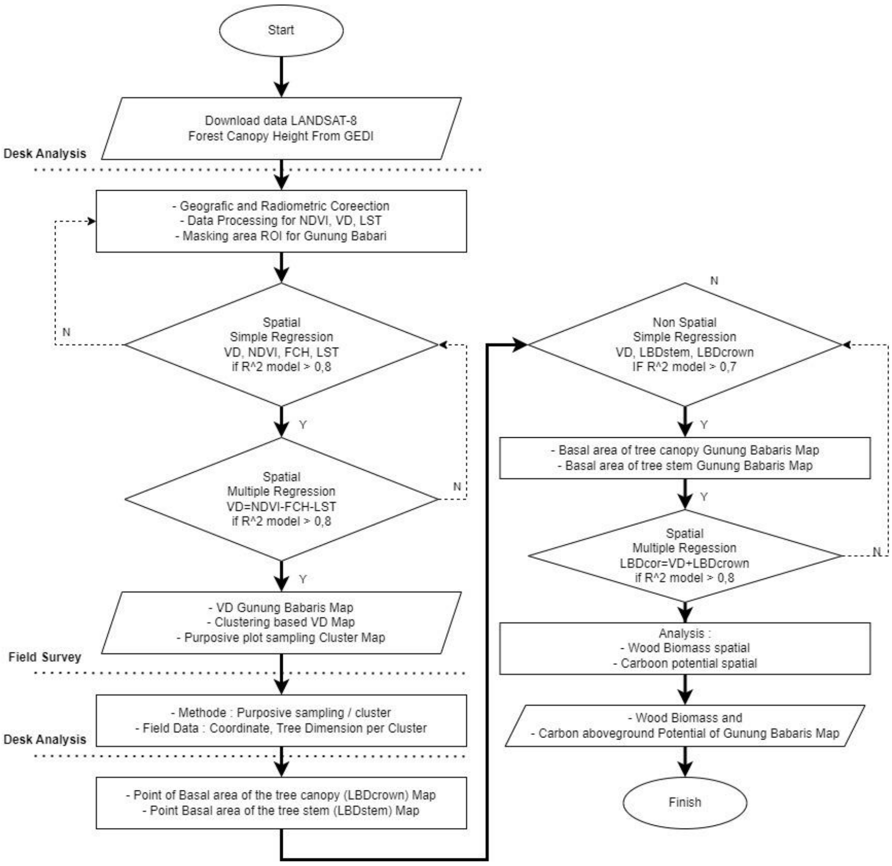

Figure 2. Research flow for analyzing soil surface carbon potential

This field data is crucial for validating the model and conducting further analysis. Once the field data collection is complete, the data is analyzed. Maps of the basal area of the tree canopy (LBDcrown) and tree stem (LBDstem) are created based on the collected data. Both simple and multiple regressions are performed with VD, LBDstem, and LBDcrown. If the R^2 value from these regressions is greater than 0.7, basal area maps are created. If the R^2 value exceeds 0.8, wood biomass and carbon potential analyses are conducted, which are then visualized as distribution maps. After completing the analysis, the model is validated by comparing the results with the field data. This validation step ensures the accuracy of the model in predicting biomass and carbon in similar regions. Finally, the results of the model are visualized on maps showing wood biomass, carbon potential, and other relevant indicators. These visualizations provide valuable information for environmental planning, management, and climate change mitigation.

4. Results and Discussion

Based on the results of the simple regression analysis conducted in this study, the relationships between the parameters VD, NDVI, LST, and FCH (see figure 3) showed correlation relationships ranging from low to high. Figure 3 shows the correlation between VD, FCH, LST, and NDVI. The relationship between LST and FCH (figure 3a) with an R^2 value of 0.3705, VD and LST (figure 3b) with an R value of 0.5743, VD and NDVI (figure 3c) with an R^2 value of 0.5656, and LST and FCH (figure 3d) with an R^2 value of 0.3705. The relationship between NDVI and LST has the highest r value. Almost 75.7% of the surface temperature conditions and 75.2% of the greenness index conditions can describe the state of stand density. Based on the above correlation values, the relationship of these four spatial parameters was continued with multiple regression analysis.

The multiple regression equation model for forest spatial density in this area is VD = 123.295486 NDVI - 0.413961 LST - 0.410253 FCH - 3.173195 with R^2 = 0.8673; RMSE = 2.6630; MAE = 2.6630; n = 17503. A positive coefficient of 123.295486 indicates that an increase in NDVI will increase VD. The higher the NDVI, the higher the VD. The negative coefficient for LST of -0.413961 indicates that an increase in surface temperature will decrease VD. The

ISSN 2723-6471

higher the LST, the lower the VD. The negative coefficient for FCH of -0.410253 indicates that an increase in forest canopy height will decrease VD. The higher the FCH, the lower the VD. The intercept is the VD value when all predictor variables (NDVI, LST, FCH) are zero. An intercept of -3.173195 indicates the starting point of vegetation density without the influence of predictor variables. This equation is useful in understanding how environmental factors such as the greenness index (NDVI), surface temperature (LST), and canopy height (FCH) affect vegetation density in the study area.

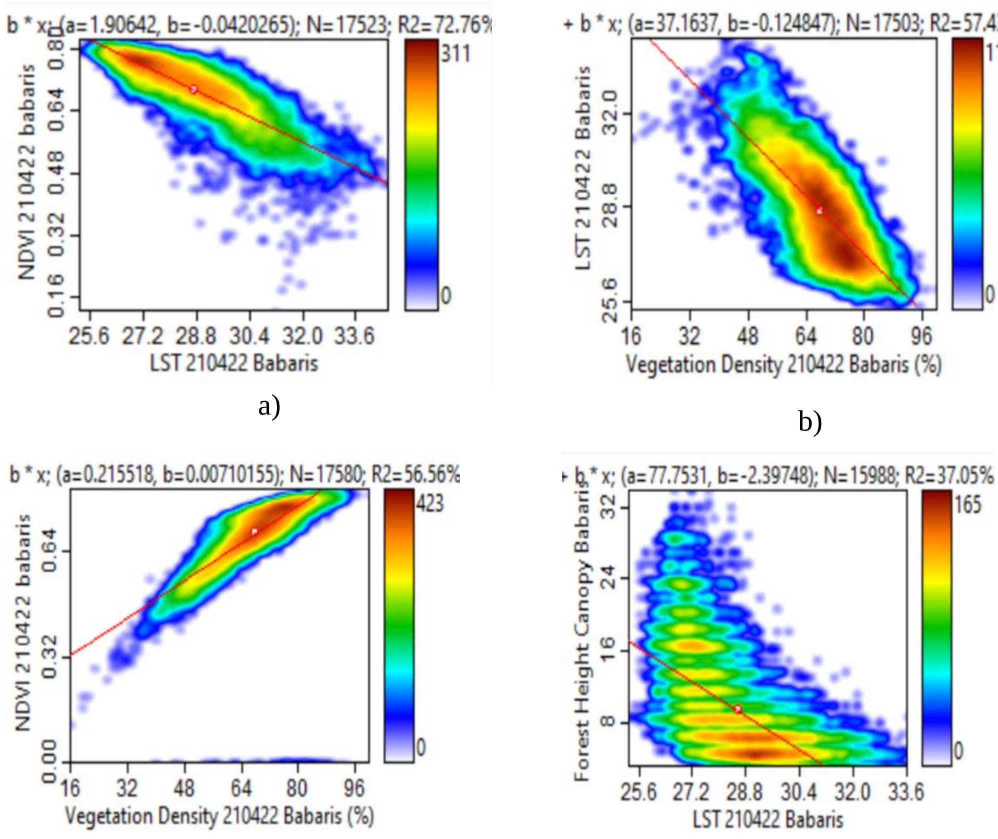

c) d)

Figure 3. Correlation between VD, FCH, LST and NDVI

From the model statistics, the coefficient of determination (R^2) of 0.8673 indicates that 86.73% of the variation in VD can be explained by the predictor variables NDVI, LST, and FCH. This indicates the model has a good fit. The Root Mean Square Error (RMSE) of 2.6630 indicates the average prediction error of the model. The lower the RMSE value, the better the model is at predicting vegetation density. The Mean Absolute Error (MAE) of 2.6630 indicates the average absolute error in the model's prediction. Like RMSE, the lower the MAE value, the better the model. The result of Spatially analysis such the VD in the Mount Babaris forest is visualized in figure 4 below.

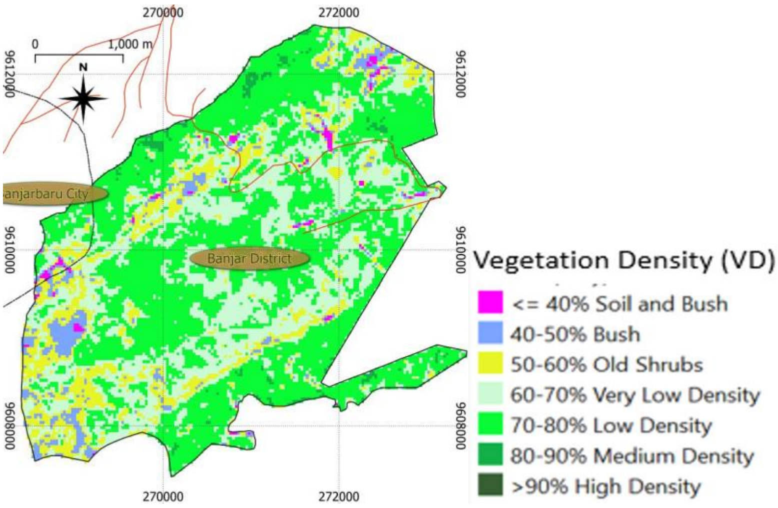

Figure 4. Prediction map of forest stand density (VD) on Mount Babaris

Figure 4 presents the predicted forest stand density map. Figure 4 illustrates the forest density and its distribution across the entire area. From this figure, it can be seen that the dominant stand density is in the range of 70-80% (low density). This observation is very consistent with field facts. To obtain more accurate data on stand density in the Mount Babaris area, a field survey was conducted. The results of the field survey data analysis and satellite data are graphically presented in figure 5 below.

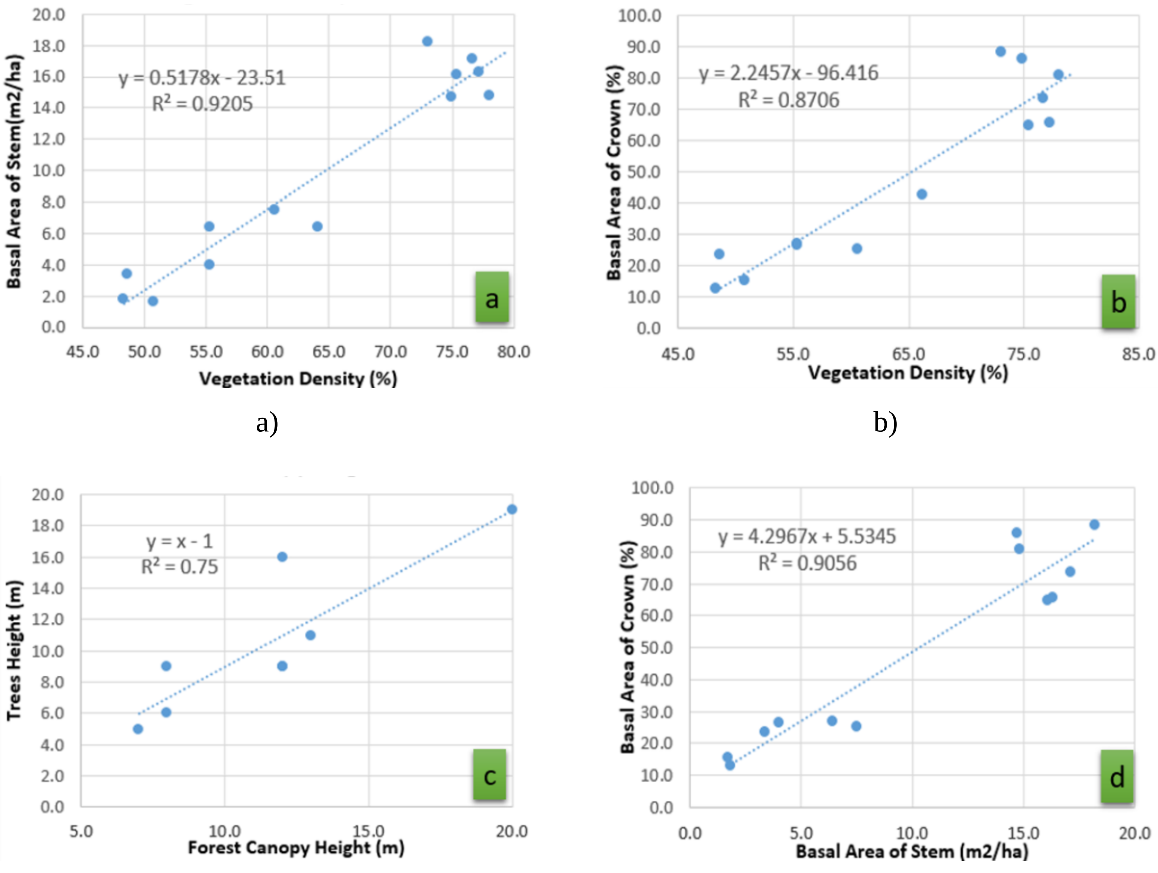

a) b)

c) d)

Figure 5. Regression relationship between field and satellite data at example locations

Figure 5 presents the simple regression relationships between survey data and satellite data at the sample locations. In figure 5a, the correlation value rrr is 0.96, in figure 5b, the correlation value rrr reaches 0.93, in figure 5c, the correlation value rrr is 0.87, and in figure 5d, the correlation value rrr is 0.95. All correlation values are above 0.8, allowing for further analysis with multiple regression. From these regression values, it can be assumed that the field data values can be approximated with the satellite data values corrected through biophysical modeling, or in other words, the satellite data values corrected through biophysical modeling can be used as a source for predicting field data.

The resulting multiple regression equation model for the spatial basal area of tree stems is LBDstemCor = 0.224811 LBDcrown + 0.001457 VD – 1.248105; R=0.9991, RMSE=0.0371. The positive coefficient of 0.224811 indicates that an increase in the basal area of the tree canopy will increase the corrected basal area of the tree stem (LBDstemcor). The larger the LBDcrownLBDcrownLBDcrown, the larger the LBDstemCorLBDstemCorLBDstemCor. The positive coefficient of 0.001457 indicates that an increase in vegetation density will increase the corrected basal area of the tree stem(LBDstemCor). The higher the VD, the larger the LBDstemCor. The intercept is the LBDstemCor value when all predictor variables (LBDcrown and VD) are zero. An intercept of -1.248105 indicates the starting point of the corrected basal area of the tree stem without the influence of predictor variables. The correlation coefficient (R) of 0.9991 indicates a very strong and nearly perfect relationship between the predictor variables (LBDcrown and VD) and the dependent variable (LBDstemCor). The RMSE of 0.0371 indicates the average prediction error of the model. This very low RMSE value indicates that the model has very high predictive accuracy, with minimal error. This equation is useful for understanding and predicting how the basal area of the tree canopy (LBDcrownLBDcrownLBDcrown) and VD contribute to the corrected basal area of the tree stem (LBDstemCor) in the study area. Visually, the results of vegetation density based on basal area (LBDstemCor) are presented in figure 6 below.

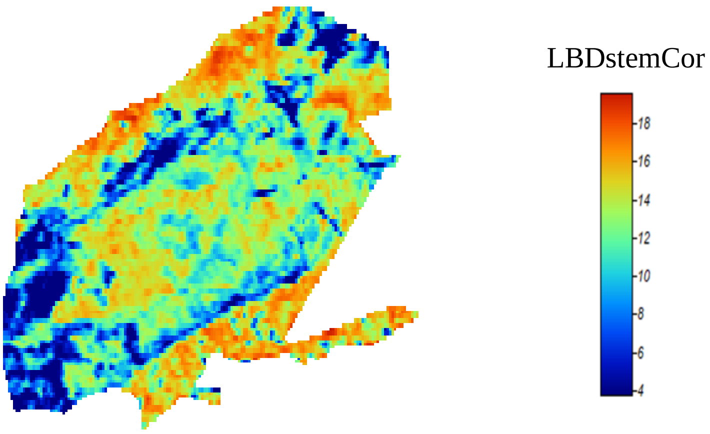

Figure 6. Potential and Distribution of Basal Area Trees (LBDstemCor) on Mount Babaris

Figure 6 presents the potential basal area of tree stems per pixel in Mount Babaris within the KHDTK ULM area. From figure 6, the range of LBDstemCorLBDstemCorLBDstemCor values can be seen from 4 to 18 m^2 per 30 x 30m pixel, according to the resolution of LANDSAT-8 pixels. Thus, the first equation, which pertains to VD, can be calculated solely through spatial analysis without fieldwork, while the second equation is based on the results of both equations above. The potential wood carbon (kg/pixel) can be calculated using the predictive model equation for Carbon Potential CPP = LBDstemCor x FCHcor x 0.7 x 680 x 1.34 x 0.47. LBDstemCor is the corrected basal area of the tree stem, which measures the basal area at the ground level. FCHcor is the corrected forest canopy height, providing vertical height information of the trees, which correlates with the amount of stored carbon. The constant 0.7 is a commonly used tree form correction factor. The constant 680 is a conversion factor to transform biomass (in volume or area units) into carbon mass in kilograms, typically used for forested areas. This equation estimates the amount of carbon stored in tree biomass in each pixel of the satellite image in the study area. The constant 0.47 is a standard conversion figure, meaning 47% of the dry biomass is carbon.

FCH and Basal Area (LBD) are important for estimating carbon potential in forest ecosystems.highlighted the relationship between mangrove canopy height and carbon stock to demonstrated the role of FCH in carbon stock and cycle analysis. Similarly, [28] emphasized FCH for estimating biomass, carbon sequestration, and forest resource assessment. [29] also discussed the importance of FCH as a key structural parameter of forests. The study by [30] addressed the use of remote LiDAR data to predict diameter distribution in temperate forests, highlighting LiDAR's potential for mapping forest characteristics. [31] discussed the growth of large old trees under climate change, highlighting the relationship between basal area increment, forest dynamics, and carbon sequestration. [31] showed

ISSN 2723-6471

that tree seed size can predict community composition and carbon storage in rainforests. The contribution of forest rehabilitation with agroforestry to carbon storage and the impact of land cover change.

The results are presented numerically and spatially as maps. Numerically, the predicted aboveground carbon potential is 179 TonC/ha. The area of Mount Babaris is approximately 1,576 ha, thus the aboveground carbon potential reaches 743,858 TonC, with a range of 743,854 to 743,939 TonC. Spatially, the aboveground carbon potential map is presented in figure 7 below.

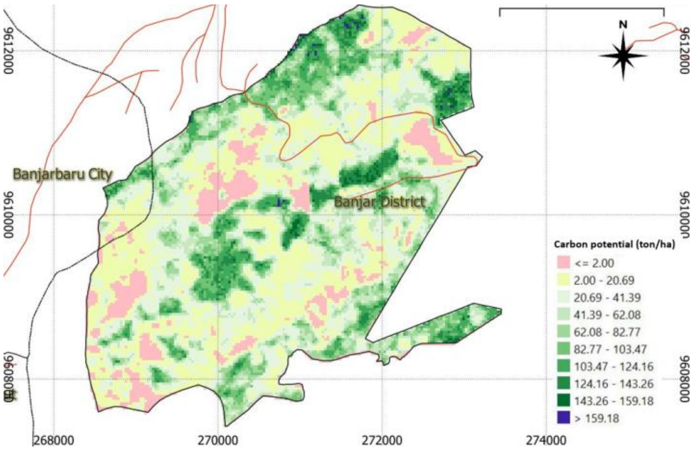

Figure 7. Map of potential and distribution of carbon above the soil surface on Mount Babaris

Figure 7 presents the predicted potential and distribution of aboveground carbon in Mount Babaris. The figure shows the potential and distribution of aboveground carbon ranging from low (≤ 2 tons/ha) to high (> 159 tons/ha) spread across the entire study area in Mount Babaris.

5. Conclusion and Recommendations

5.1. Conclusion

The equation model analysis results based on satellite data show that the vegetation density (VD) can be calculated using the equation: VD = 123.295486 × NDVI - 0.413961 × LST - 0.410253 × FCH - 3.173195. This equation is validated through field measurements, demonstrating that 86.73% of the variation in vegetation density can be explained by NDVI, LST, and FCH. Additionally, the equation model analysis results based on a combination of satellite and field data show that the basal area of the stem (LBDstemCor) can be determined using the equation: LBDstemCor = 0.007645 × LBDcrown + 0.034348 × VD - 1.575439. With an R^2 value of 0.9564, this equation shows high accuracy in predicting the basal area of tree stems based on crown basal area and vegetation density. To predict the carbon potential (CPP) in kilograms per pixel, the equation used is: CPP = LBDstemCor × FCHcor × 0.7 × 680 × 1.34 × 0.47. This equation estimates the amount of carbon stored in tree biomass per pixel by integrating the corrected basal area of tree stems and forest canopy height. Overall, the above-ground carbon potential in the entire area of Gunung Babaris (1,576 ha) is estimated to be between 607,767.55 and 607,829.54 tons of carbon. By presenting these equations separately and clearly, the readability and understanding of the biophysical model are significantly improved, ensuring that each component of the model is comprehensible and logically structured.

5.2. Recommendations

Future research should focus on refining the biophysical models to improve the accuracy of vegetation density and carbon potential predictions. Integrating more advanced remote sensing technologies such as LiDAR and high-resolution satellite imagery could enhance the precision of canopy height and basal area measurements. Additionally, expanding field surveys to include a larger and more diverse range of sampling plots will help validate the models more robustly and account for variability across different forest types and conditions. Further studies should also explore the temporal dynamics of carbon sequestration by incorporating time-series data to monitor changes in forest biomass and carbon stocks over time. This will provide valuable insights into the long-term impacts of environmental changes and management practices on forest ecosystems. Collaborative efforts with local communities and

ISSN 2723-6471

stakeholders are recommended to implement sustainable forest management strategies that optimize carbon storage while preserving biodiversity and ecosystem services.

6. Declarations

6.1. Author Contributions

Conceptualization: A.J., I.S., L.T., and M.; Methodology: I.S.; Software: A.J.; Validation: A.J., I.S., L.T., and M.; Formal Analysis: A.J., I.S., L.T., and M.; Investigation: A.J.; Resources: I.S.; Data Curation: I.S.; Writing Original Draft Preparation: A.J., I.S., L.T., and M.; Writing Review and Editing: I.S., A.J., L.T., and M.; Visualization: A.J.; All authors have read and agreed to the published version of the manuscript.

6.2. Data Availability Statement

The data presented in this study are available on request from the corresponding author.

6.3. Funding

The authors received no financial support for the research, authorship, and/or publication of this article.

6.4. Institutional Review Board Statement

Not applicable.

6.5. Informed Consent Statement

Not applicable.

6.6. Declaration of Competing Interest

The authors declare that they have no known competing financial interests or personal relationships that could have appeared to influence the work reported in this paper.

References

[1] H. D. Nirwana, A. R. Saidy, G. M. Hatta, and A. Nugroho, "Design of a Green City with Lower Carbon Based on Vegetation in Banjarbaru using Sentinel-2," *J. Appl. Data Sci*., vol. 5, no. 2, pp. 583–599, 2024, doi: 10.47738/jads.v5i2.218.

[2] M. J. Kryzanek, *Debates, Differences and Divisions the 25 Issues That Shape American Politics*, 1st Edition., vol. 1. London England, United Kingdom: Routledge, 2016, doi: 10.4324/9781315664378-10.

[3] L. Taati, Sunardi, I. Syauqiah, and A. Jauhari, "Assessing Drought Risk in Forest Zones Near Coal Mines with Temperature Vegetation Dryness Index," *J. Appl. Data Sci*., vol. 5, no. 2, pp. 559–570, 2024, doi: 10.47738/jads.v5i2.220.

[4] Munsyi, A. Nugroho, A. Jauhari, and M. R. Faisal, "Urban Heat Island Spatial Model for Climate Village Program Planning," *J. Appl. Data Sci*., vol. 5, no. 2, pp. 546–558, 2024, doi: 10.47738/jads.v5i2.223.

[5] R. Amandanu, B. I. Arijuddin, A. Jauhari, and I. A. Ariseno, "Toponymy analysis as geosocial cultural approach on disaster mitigation studies in Sumberagung Village Pracimantoro District Wonogiri Regency," *IOP Conf. Ser. Earth Environ. Sci.*, vol. 1314, no. 1, pp. 1-9, 2024, doi: 10.1088/1755-1315/1314/1/012122.

[6] A. Nugroho, and U. B. L. Utami, "The Local Wisdom of the Paramasan Dayak Tribe in Environmental Management," *Environ. Ecol. Res.*, vol. 11, no. 5, pp. 859–872, 2023, doi: 10.13189/eer.2023.110514.

[7] B. A. Alotaibi, "Dynamics and Determinants of Farmers' Perceptions About Causes and Impacts of Climate Change on Agriculture in Saudi Arabia: Implications for Adaptation, Mitigation, and Sustainability," *Atmosphere (Basel)*., vol. 14, no. 6, pp. 1-17, 2023, doi: 10.3390/atmos14060917.

[8] H. O. Stanley, P. T. Bestmann, and C. J. Ugboma, "Public Perception of Climate Change Impact on Human Health in Trans Amadi Area of Port Harcourt, Rivers State, Nigeria," *Asian J. Environ. Ecol*., vol. 14, no. 1 pp. 59–65, 2021, doi: 10.9734/ajee/2021/v14i130197.

[9] F. Köprülü, O. A. M. Hamad, and A. Kiraz, "Perceptions of Libyans Towards Climate Change," *Int. J. Ecosyst. Ecol. Sci*., vol. 13, no. 2, pp. 37–44, 2023, doi: 10.31407/ijees13.205.

[10] K. Hayes, G. Blashki, J. Wiseman, S. Burke, and L. Reifels, "Climate Change and Mental Health: Risks, Impacts and Priority Actions," *Int. J. Ment. Health Syst.*, vol. 12, no. 281, pp. 12-27, 2018, doi: 10.1186/s13033-018-0210-6.

[11] A. Price, E. C. Jones, and F. Jefferson, “Vertical Greenery Systems as a Strategy in Urban Heat Island Mitigation,” *Water, Air, Soil Pollut.*, vol. 226, no. 8, pp. 247-259, 2015, doi: 10.1007/s11270-015-2464-9.

[12] B. Sajan, S. Kanga, S. K. Singh, V. N. Mishra, and B. Durin, “Spatial variations of LST and NDVI in Muzaffarpur district, Bihar using Google earth engine (GEE) during 1990-2020,” *J. Agrometeorol.*, vol. 25, no. 2 SE-Research Paper, pp. 262–267, May 2023, doi: 10.54386/jam.v25i2.2155.

[13] M. Sharma, P. Bangotra, A. S. Gautam, and S. Gautam, “Sensitivity of Normalized Difference Vegetation Index (NDVI) to Land Surface Temperature, Soil Moisture and Precipitation Over District Gautam Buddh Nagar, UP, India,” *Stoch. Environ. Res. Risk Assess.*, vol. 36, no. 8, pp. 1779-1789, 2021, doi: 10.1007/s00477-021-02066-1.

[14] A. Grover and R. B. Singh, “Analysis of urban heat island (Uhi) in relation to normalized difference vegetation index (ndvi): A comparative study of delhi and mumbai,” *Environ. - MDPI*, vol. 2, no. 2, pp. 125–138, 2015, doi: 10.3390/environments2020125.

[15] S. Kandel, B. Gyawali, J. Sandifer, S. Shrestha, and S. Upadhaya, “Assessment of Urban Heat Islands (UHIs) Using Satellite-Derived Normalized Difference Vegetation Index (NDVI), and Land Surface Temperature (LST) in Three Metropolitan Cities of Nepal,” *Banko Janakari*, vol. 32, no. 2, pp. 37–51, 2022, doi: 10.3126/banko.v32i2.50895.

[16] D. Sun and M. Kafatos, “Note on the NDVI-LST relationship and the use of temperature-related drought indices over North America,” *Geophys. Res. Lett.*, vol. 34, no. 24, pp. 1-12, 2007, doi: 10.1029/2007GL031485.

[17] S. Guha, H. Govil, and P. Diwan, “Monitoring LST-NDVI Relationship Using Premonsoon Landsat Datasets,” *Adv. Meteorol.*, vol. 12, no. 2, pp. 1–15, 2020, doi: 10.1155/2020/4539684.

[18] Y. Deng, “Relationship Among Land Surface Temperature and LUCC, NDVI in Typical Karst Area,” *Sci. Rep.*, vol. 8, no. 641, pp. 1–12, 2018, doi: 10.1038/s41598-017-19088-x.

[19] I. Sandholt, K. Rasmussen, and J. Andersen, “A simple interpretation of the surface temperature/vegetation index space for assessment of surface moisture status,” *Remote Sens. Environ.*, vol. 79, no. 2, pp. 213–224, 2002.

[20] L. K. Torres Gil, D. Valdelamar Martínez, and M. Saba, “The Widespread Use of Remote Sensing in Asbestos, Vegetation, Oil and Gas, and Geology Applications,” *Atmosphere (Basel).*, vol. 14, no. 1, pp. 1-35, 2023, doi: 10.3390/atmos14010172.

[21] S. Jain, S. Sannigrahi, S. Sen, S. Bhatt, S. Chakraborti, and S. Rahmat, “Urban heat island intensity and its mitigation strategies in the fast-growing urban area,” *J. Urban Manag.*, vol. 9, no. 1, pp. 54–66, 2020, doi: 10.1016/j.jum.2019.09.004.

[22] N. Li and J. Wang, “Comprehensive Eco-Environment Quality Index Model with Spatiotemporal Characteristics,” *Sensors*, vol. 22, no. 24, pp. 1- 31, 2022, doi: 10.3390/s22249635.

[23] A. W. Hastuti, K. I. Suniada, and F. Islamy, “Carbon Stock Estimation of Mangrove Vegetation Using Remote Sensing in Perancak Estuary, Jembrana District, Bali,” *Int. J. Remote Sens. Earth Sci.*, vol. 14, no. 2, pp. 137-149, 2018, doi: 10.30536/j.ijreses.2017.v14.a2841.

[24] S. S. Rijal, T. D. Pham, S. Noer’Aulia, M. I. Putera, and N. Saintilan, “Mapping Mangrove Above-Ground Carbon Using Multi-Source Remote Sensing Data and Machine Learning Approach in Loh Buaya, Komodo National Park, Indonesia,” *Forests*, vol. 14, no. 1, pp. 1-20, 2023, doi: 10.3390/f14010094.

[25] B. Usmanov, “Remote Sensing Monitoring on the Territory of the Volga Carbon Polygon (Republic of Tatarstan, Russia),” *E3s Web Conf.*, vol. 463, no. 1, pp. 2021-2034, 2023, doi: 10.1051/e3sconf/202346302021.

[26] I. G. A. I. Mahasani, T. Osawa, I. W. S. Adnyana, A. A. M. A. P. Suardana, and Chonnaniyah, “Carbon Stock Estimation and Mapping of Mangrove Forest Using ALOS-2 PALSAR-2 in Benoa Bay Bali, Indonesia,” *Iop Conf. Ser. Earth Environ. Sci.*, vol. 944, no. 1, pp. 12044-12057, 2021, doi: 10.1088/1755-1315/944/1/012044.

[27] Y. Chen, J. P. Guerschman, Z. Cheng, and L. Guo, “Remote Sensing for Vegetation Monitoring in Carbon Capture Storage Regions: A Review,” *Appl. Energy*, vol. 240, no.10, pp. 312–326, 2019, doi: 10.1016/j.apenergy.2019.02.027.

[28] A. Rajib, G. R. Evenson, H. E. Golden, and C. R. Lane, “Hydrologic Model Predictability Improves With Spatially Explicit Calibration Using Remotely Sensed Evapotranspiration and Biophysical Parameters,” *J. Hydrol.*, vol. 567, no.10, pp. 668–683, 2018, doi: 10.1016/j.jhydrol.2018.10.024.

[29] D. Rocchini, “Uncertainty in Ecosystem Mapping by Remote Sensing,” *Comput. Geosci.*, vol. 50, no.2, pp. 128–135, 2013, doi: 10.1016/j.cageo.2012.05.022.

[30] P. J. Leitão, “From Sample to Pixel: Multi-scale Remote Sensing Data for Upscaling Aboveground Carbon Data in Heterogeneous Landscapes,” *Ecosphere*, vol. 9, no. 8, pp. 1-14, 2018, doi: 10.1002/ecs2.2298.

[31] R. Rahmadanti, A. Jauhari, D. M. Asy’ari Program, and S. Kehutanan, “Distribution of Urban Heat Island at Banjarbaru Using Remote Sensing,” *J. Sylva Sci.*, vol. 05, no. 2, pp. 194–202, 2022.